REFLECTANCE AND FLUORESCENCE CONFOCAL MICROSCOPE FOR IMAGING OF THE MOUSE COLON

A Thesis

by

MEAGAN ALYSSA SALDUA

Submitted to the Office of Graduate Studies of
Texas A&M University
in partial fulfillment of the requirements for the degree of

MASTER OF SCIENCE

December 2010

Major Subject: Biomedical Engineering

REFLECTANCE AND FLUORESCENCE CONFOCAL MICROSCOPE FOR IMAGING OF THE MOUSE COLON

A Thesis

by

MEAGAN ALYSSA SALDUA

Submitted to the Office of Graduate Studies of
Texas A&M University
in partial fulfillment of the requirements for the degree of

MASTER OF SCIENCE

Approved by:

Chair of Committee,	Kristen Carlson Maitland
Committee Members,	Javier Jo
	Robert Chapkin
Head of Department,	Gerard L. Coté

December 2010

Major Subject: Biomedical Engineering

ABSTRACT

Reflectance and Fluorescence Confocal Microscope for Imaging of the Mouse Colon.

(December 2010)

Meagan Alyssa Saldua, B.S., Angelo State University

Chair of Advisory Committee: Dr. Kristen Carlson Maitland

Many Americans are afflicted with inflammation of the colon. They are also at a higher risk of developing colon cancer. Confocal microscopy of bulk epithelial tissue has the potential to provide information on tissue structural properties that may be lost in the fixation and slicing procedures required for histopathology. Optical sectioning provides images in three dimensions capturing the organizational structure of cells and colon crypts throughout the entire colon. I have constructed a custom built fluorescence and reflectance confocal microscope for imaging molecular and morphological changes associated with development of inflammation in a mouse model.

A confocal microscope is a point scanning system that removes out of focus light by placing a pinhole aperture in the conjugate image plane located in front of the detector. We have two sources, 488 nm and 811 nm, for fluorescence and reflectance imaging, respectively. A polygon scanning mirror and a galvanometer scanning mirror allow for a variable scan rate between 8 and 15 fps. The lateral resolution of the system is approximately 3 μm with an axial resolution of 6 μm and 4 μm for reflectance and fluorescence mode, respectively.

As colon tissue becomes inflamed, there is a distinct change in the structure and architecture of the tissue. The colon crypts are no longer uniform in size or distribution throughout the tissue. Having a large field of view of $1mm^2$ allows for many colon crypts to be visualized within a single frame. Histology was performed on the same tissue imaged for the inflammatory study confirming the constructed confocal microscope's ability to characterize inflamed tissue and the potential use for guided biopsy.

Mosaicing, or image tiling, is an imaging technique that stitches single frames together to produce a much larger field of view. An extended frame with 1 mm x 2 cm field of view is achieved within seconds. This extended frame would allow mosaicing of the entire mouse colon much faster than conventional methods without loss of resolution.

The acquired confocal images of colon tissue demonstrate the microscope's ability to resolve cell nuclei lining the colon crypts within a relatively large field of view.

ACKNOWLEDGEMENTS

I would like to thank my committee chair, Dr. Kristen Maitland, and my committee members, Dr. Javier Jo, and Dr. Robert Chapkin, for their guidance and support throughout the course of this research.

I also want to thank my mother and father for their endless encouragement.

TABLE OF CONTENTS

Page

LIST OF FIGURES

Page

LIST OF TABLES

1. INTRODUCTION

1.1 Motivation

Those experiencing ulcerative colitis or Crohn's disease have an increased risk for developing colorectal cancer; therefore, there is an assumption that chronic inflammation causes cancer [1]. Ulcerative colitis is reported as inflammation in the colon that is restricted to the mucosa or innermost layer [2]. Crohn's disease includes the small intestine, colon, and other surrounding organs [3]. Currently, it is recommended that patients experiencing high risk of developing colon cancer are voluntarily subjected to colonoscopy evaluations. In many cases, this results in the need for multiple biopsies and in severe cases, surgery. Targeting an ideal location to biopsy during a colonoscopy can be difficult due to the small field of view and poor resolution. A random biopsy may not necessarily represent the condition of the whole colon if collagenous colitis is present [4]. Confocal microscopy can perform an optical biopsy in vivo. This means that the tissue does not have to be removed from the body, fixed, or sliced. Instead, a virtual histology-type image is visualized almost instantaneously on a computer monitor. This form of imaging shows potential of being used as an instrument for guided biopsy in a clinical setting [5].

It is possible to model human colitis in healthy rodents by treating them with dextran sulfate sodium in their drinking water [6]. The longer the disease duration, the increased rate of neoplasia exhibited. When used in conjunction with azoxymethane, the mice can develop colon cancer [7]. Using confocal microscopy as an optical biopsy tool,

---

This thesis follows the style of Biomedical Optics Express.

there is an opportunity to image bulk tissue with higher resolution compared to traditional microscopy. There is also a potential to aid pathologists to a quicker diagnosis of the state of the tissue while viewing confocal images on a monitor in near-real time.

1.2 Research Goals

The images from a bench top confocal microscope to a portable fiber-based system exhibit some differences in resolution and penetration depth [8]. A non-fiber based system can have better resolution, larger field of view, and deeper imaging depth within excised tissue than a fiber-based system.

The objective of this research is to evaluate the ability of a dual-mode confocal microscope to characterize structural and molecular changes in mouse colon tissue as inflammation and cancer develop. The first specific aim of this work is to design and build a dual-mode reflectance and fluorescence confocal microscope based on specific design requirements for imaging bulk colon tissue. The second specific aim is to image colon tissue of healthy mice and mice with induced inflammatory bowel disease. The acquired confocal images will be compared to corresponding histology images.

1.3 Thesis Overview

In my thesis, I will present the design requirements for the reflectance and fluorescence confocal microscope tailored to a mouse colon application. I will then show the evaluation of my system's performance such as resolution, field of view, and some preliminary data acquired from normal mouse colon tissue imaged in fluorescence mode. Next, I will present confocal images taken of normal and inflamed mouse tissue in both reflectance and fluorescence mode along with corresponding histology images. Moving

the sample on the stage in a single axis in conjunction with the polygon mirror provides confocal images with an extended field of view without loss of resolution. Lastly, I will summarize the results of my work and provide a conclusion with goals for the continuation of this project for my dissertation.

2. BACKGROUND

2.1 Inflammation and Colorectal Cancer

An estimated 2 million Americans are afflicted with bowel inflammation, a recurring condition that is not fully understood. Although studies have shown a direct relationship between inflammation and colon cancer, early cancer detection remains a challenge. One in 19 Americans are at risk of developing colon cancer in their lifetime [9]. After 7 years of inflammation, the risk of developing colon cancer increases by 0.5-1% every year [3]. Patients experiencing inflammatory bowel disease often report symptoms such as abdominal pain, diarrhea, rectal bleeding, weight loss, fever, and fatigue [10].

Normal colon tissue is very structured, exhibiting a hexagonal pattern. Colon crypts have a uniform distribution and are covered by a homogenous layer of epithelial cells. As new tissue generates and tumors develop, the crypts appear star shaped and the vessels begin to leak causing the structured architecture to become distorted and irregular with a loss of crypts and epithelial cells [11]. The localization of dysplasia or cancer is noted to be 20% at the proximal end of the colon, 44% in the middle, and 36% at the distal end [1], therefore affecting the entire colon.

Colon cancer typically begins as a benign polyp in the colon. At stage 0, the tumor is typically removed during a routine colonoscopy evaluation as it has not yet invaded surrounding tissue [9]. In stage 1, the tumor is no longer just at the surface and has now invaded more tissue layers within the colon. As the cancer progresses to stage 2, nearby tissue is now affected and radiation therapy may be recommended for the patient. Stages 3 and 4 are more advanced. First, the cancer spreads to the lymph nodes and chemotherapy treatments are recommended. At stage 4, the cancer has spread to surrounding organs within the body and sometimes parts of organs must be removed.

Histopathology is the most common technique used to evaluate and diagnose colon tissue after completion of a biopsy during a colonoscopy [12]. Histology provides images of cellular and tissue structure after a biopsy of the colon is performed during a colonoscopy. The tissue must be fixed, sliced, and stained before it is evaluated by the pathologist. This is a time intensive process causing patient discomfort. Artifacts can be introduced during tissue preparation causing a misrepresentation of the tissue. Figure 1 shows an en face histology image of normal colon tissue. Colonic features such as colon crypts vary from 75 – 150 μm [13].

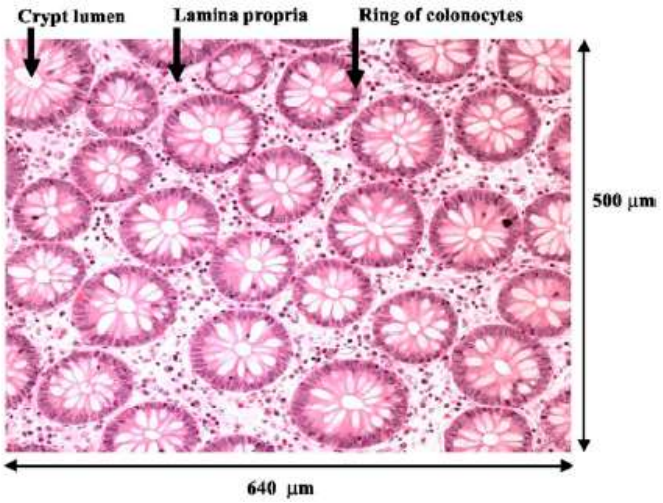

Fig. 1. En face histology image of normal colon tissue noting architecture of colon tissue [13]. The tissue is stained with hematoxylin and eosin to provide contrast. Hematoxylin stains the nuclei blue and eosin stains the surrounding cytoplasm pink.

Some studies have been performed comparing histology images to confocal images as a means to determine how useful confocal microscopy will be as a guided biopsy tool [14]. In Figure 2, the images in the left column are histology images and in the right column, confocal images. The top row is normal tissue, and the bottom row is inflamed tissue. In the histology image of normal tissue, the crypts appear uniform in size and distribution. In the inflamed tissue, the crypts vary in size and exhibit distortion. The corresponding confocal images correlate well with the histology images indicating that confocal microscopy has the potential to aid in tissue diagnosis. The images are 500 μm square, acquired at 1.4 fps. The maximum penetration depth achieved during imaging was 250 μm with an axial resolution of 10 microns.

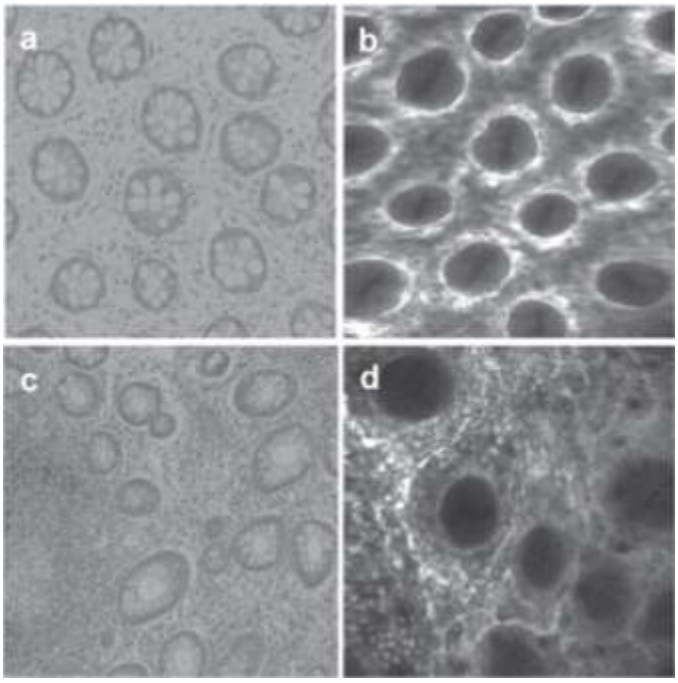

Fig. 2. Histology and fluorescence confocal images comparing normal and inflamed colon tissue to corresponding histology images [14]. In the confocal images, the normal and inflamed tissues are stained with 200 μg of fluorescein.

As normal tissue becomes inflamed, I expect to see a change in the architecture and structure of the colon crypts. The colon crypts will not be uniform in size or distribution throughout the tissue. As precancerous tissue develops, I predict there will be abnormal cell growth and a production of nuclei throughout the colon tissue. This will be indicative in confocal images by the bright clumping of nuclei causing the nuclear to cytoplasmic ratio to increase. Once the tissue is cancerous, a total loss in architecture should be exhibited including loss of epithelial cells and colon crypts as the cancer spreads to surrounding tissue and organs in the body.

2.2 Confocal Microscopy

Confocal microscopy can image bulk tissue in three dimensions with higher levels of resolution and contrast [15] than widefield microscopy. In contrast to the physical sectioning and two dimensional imaging of traditional histology, confocal imaging allows optical sectioning of bulk tissue, enabling acquisition of three dimensional images of intact tissue.

Confocal microscopy uses a point source illumination that is focused onto a sample and a point detector for collection of signal. Figure 3 shows a simple schematic of confocal microscopy [16].

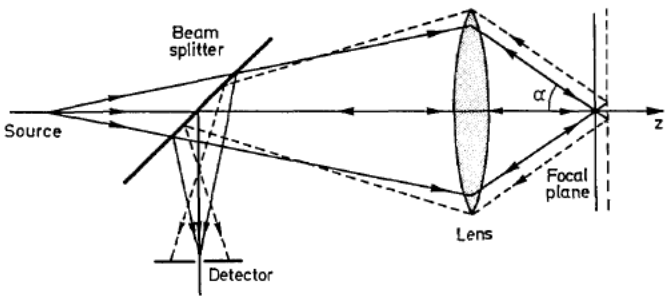

Fig. 3. Simple confocal schematic showing the light path of a confocal microscope [16].

In Figure 3, a point source is used as the illumination source. If imaging in reflectance mode, the light passes through a beam splitter since the entire signal coming from the focal plane within the sample is collected. If imaging in fluorescence mode, the beam splitter is replaced with a dichroic mirror so only the fluorescence signal is detected, not the illumination source. The light is focused to a plane within the sample

and the reflectance or fluorescence signal is collected by the same lens and reflects off of the beam splitter of dichroic mirror.

High-resolution confocal reflectance and fluorescence images of tissue are collected by placing a pinhole in front of the detector to reject light coming from out of focus planes within the sample. In order to create a two dimensional image, the point source is scanned across the sample using a scanning technique. The sample is never completely illuminated at one time, only a single point. This allows images to be seen in near real-time. Moving the sample in the third axial dimension builds a three-dimensional tomographic image. Constructed benchtop confocal microscopes report image depths up to 250 μm in reflectance mode, allow imaging of epithelial tissue that lines the cavities of organs in the body. A field of view (FOV) of 300 x 300 μm has been achieved [15, 17]. A larger field of view is typically achieved by stitching images together using a confocal mosaicing post-processing technique [18] in an image processing software such as Matlab. The Leica TCS SP2 AOBS commercial confocal microscope is reported as capable of achieving a FOV of 750 x 750 μm and a maximum imaging depth of 420 μm [15]. Modified commercial systems are reported to have a 430 μm FOV [19]. The in vivo confocal scanning laser microscope from Milind Rajadhyaksha's lab has reported a maximum penetration depth of 450 μm in oral mucosa [20] and was designed to have a FOV of 250 x 250 μm when using a 40x 0.6 NA dry objective lens from Olympus [21]. This system has been modified to additionally perform multiphoton imaging. Imaging the full epithelial layer is important because if precancer is detected in an early stage, the chance of developing cancer can be

greatly reduced. One of the tradeoffs for having better resolution is typically a smaller field of view. By custom designing a benchtop confocal microscope with a large field of view, more information about the interrogated tissue is acquired at a much faster speed without the need for post-processing techniques such as mosaicing.

The resolution of a confocal microscope indicates the microscope's capability to separate two closely spaced points. The point spread function (PSF) of a system characterizes a system's response to a point source of light. When light is focused to a point, an Airy pattern is formed by diffraction as light passes through the circular aperture of the lens. The lateral resolution, using the PSF in the lateral plane, is defined as the radius of the first dark ring around the Airy Disk and is given by Eq. (1) [22],

$$r_{Airy} = \frac{0.61\lambda}{NA_{obj}} \tag{1}$$

where λ represents the wavelength of the illumination source and NA_{obj} is the numerical aperture of the microscope objective. Lateral resolution of a confocal microscope is improved by decreasing the size of the pinhole, but there is a tradeoff when choosing the optimal pinhole size. A smaller pinhole will provide better resolution, but decrease the amount of signal detected. A larger pinhole sacrifices resolution in order to detect more signal.

The axial resolution is defined as the full width half maximum of the PSF in the axial plane and is given by Eq. (2) [23],

$$z_{axial} = \frac{1.4 \cdot \lambda \cdot n}{\left(NA_{obj}\right)^2} \tag{2}$$

where n represents the index of refraction of the object medium used.

A study was performed to determine the optimal pinhole size without having to sacrifice signal or resolution [16]. This method is applicable to many optical imaging systems by converting the axial resolution equation and pinhole radius to dimensionless optical units. The optimal pinhole size can be determined based on the wavelength of light and numerical aperture of the objective used. Eq. (3) represents the normalized pinhole radius, v_p as a function of the pinhole radius, r_p, wavelength, λ, and the numerical aperture of the objective, NA_{obj}.

$$v_p = \frac{2\pi}{\lambda}(NA_{obj})r_p \tag{3}$$

Eq. (4) represents the normalized axial position as a function of the axial position, z, and the quarter angle of the NA instead of the half angle.

$$u = \frac{8\pi}{\lambda}\left[n\sin\left(\frac{\alpha}{2}\right)\right]^2 z \tag{4}$$

Figure 4 demonstrates the half-width of the image, $v_{1/2}$, as a function of the normalized detector pinhole radius, v_p.

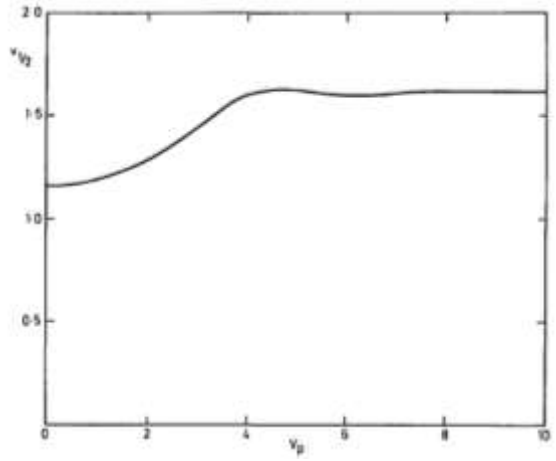

Fig. 4. Half-width, $v_{1/2}$, as a function of detector pinhole size, v_p [16].

This plot represents the lateral resolution of a system. For large v_p, the lateral resolution is comparable to traditional microscopy. As v_p is decreased below a value of 4, lateral resolution ($v_{1/2}$) is improved. For v_p=0, no signal is permitted to the detector.

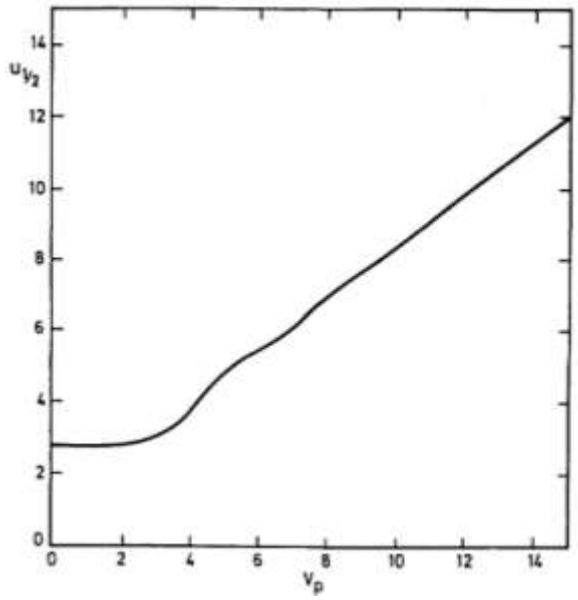

Fig. 5. Half-width, $u_{1/2}$, as a function of detector pinhole size, v_p [16].

Figure 5 represents the axial resolution of an imaging system. For v_p less than 2.5, the half-width is fairly constant; therefore a larger pinhole up to $v_p = 2.5$ will allow more signal to reach the detector without sacrificing resolution. Ideally, a pinhole size, v_p, of less than or equal to 2.5 is chosen.

2.3 Imaging Colon Tissues with Confocal Microscopy

2.3.1 Reflectance Confocal Microscopy

After applying 6% acetic acid, a process known as aceto-whitening of tissue, the nuclei appear much brighter in reflectance confocal imaging than autofluorescence imaging, and this method provides enough contrast for a quantitative study of features within epithelial tissue [24]. Studies have shown that reflectance confocal microscopy is capable of differentiating normal and dysplastic cervical tissue ex vivo [25]. A quantitative review was performed by determining the nuclear to cytoplasmic ratio and a qualitative study done using untrained observers to diagnosis the biopsies. Reflectance confocal microscopy reveals morphology of tissue and can image architectural differences between normal and inflamed mouse colon tissue [14]. In normal colonic mucosa, the cell membrane is highly reflective, while the goblet cells lining the inside of the colon crypts are not reflective causing the colon crypts to appear as black holes [26].

2.3.2 Fluorescence Confocal Microscopy

Fluorescence confocal microscopy reveals morphological changes in colonic tissue by utilizing fluorescent stains. Acridine orange (AO) is a nucleic stain that is excited at 488 nm and emits at 530 nm. Studies have shown that this fluorophore

sufficiently stains the nuclei surrounding colon crypts [27]. Colon crypts appear as black holes in confocal images. In normal rat colon tissue, epithelial cells surrounding colon crypts are clearly resolved, but after 3 days of DSS treatment, morphological changes in the colon crypts are seen. The crypts exhibit a wider spacing and there is epithelial cell loss at the surface of the tissue. After 5 days of DSS treatment, there is a loss in fluorescent signal as the number of epithelial cells at the surface is further reduced. At day 7 of treatment, crypt distortion is noted along with the loss of colon crypts in some areas. Additionally, fluorescence confocal microscopy has the potential to image biochemical changes in the tissue using endogenous fluorophores such as collagen, elastin, flavin adenine dinucleotide (FAD) and nicotinamide adenine dinucleotide (NADH) [28-29].

3. DESIGN, CONSTRUCTION, AND CHARACTERIZATION OF THE DUAL-MODE CONFOCAL MICROSCOPE

3.1 Design Requirements

I have designed and constructed a bench top combined fluorescence and reflectance confocal microscope to compare the imaging capability of these two techniques to detect changes in tissue architecture and cellular structure of colon tissue.

The design requirements were chosen based on the application of the microscope and are listed in Table 1 below.

Table 1 Confocal microscope design requirements

Parameter	**Reflectance**	**Fluorescence**
Illumination Wavelength	800 – 850 nm	350 - 600 nm
Lateral Resolution	< 1 μm	< 1 μm
Axial Resolution	< 3 μm	< 2 μm
Field of View	> 250 x 250 μm	> 250 x 250 μm
Penetration Depth	>300 μm	>150 μm
Acquisition Rate	5 – 30 fps, variable	5 – 30 fps, variable

The illumination wavelengths were chosen based on tissue optical properties and the types of fluorescent stains chosen for imaging. For confocal fluorescence imaging, an illumination wavelength of 488 nm was chosen for use with Acridine Orange (AO). Acridine Orange is excited at 488 nm and emits fluorescent signal at 530 nm. For confocal reflectance imaging, an illumination wavelength of 811 nm was chosen to reveal morphological features of the tissue. This near-infrared (NIR) wavelength is common for reflectance imaging because the light will penetrate deeper into the tissue and there is less absorption and scattering than visible wavelengths. If a longer illumination wavelength was chosen in the NIR range, the light may be able to travel further within the tissue, but resolution is sacrificed.

The lateral and axial resolutions were selected so that nuclei may be resolved and thin optical sectioning is achieved in the axial plane. It is desirable to image at least several colon crypts within a single frame; therefore, a field of view greater than 250 x 250 μm is ideal. The imaging penetration depth will vary depending on the light source used and the type of sample imaged.

Acquisition of images in near-real time and near video rate will allow the operator to view and scan the sample almost instantaneously on a computer monitor.

3.2 System Design

Figure 6 depicts a schematic of the constructed confocal microscope.

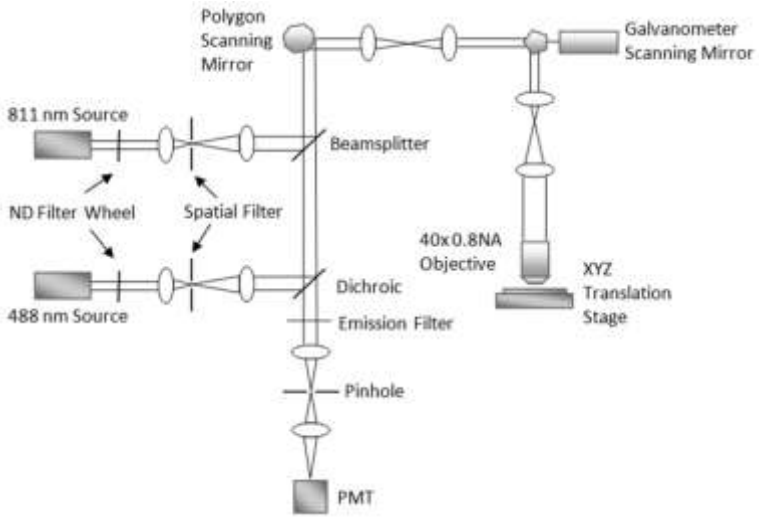

Fig. 6. Reflectance and fluorescence confocal microscope schematic showing the light path for the 811 nm and 488 nm illumination sources.

The bench top system currently has two illumination lasers: a 40 mW, 488 nm (PC14717, Newport, Santa Clara, CA) diode-pumped solid-state (DPSS) laser for fluorescence imaging and a 120 mW, 811 nm (DL808-120-O, CrystaLaser, Reno, NV) DPSS laser for reflectance imaging. They are continuous wave lasers that pass through variable absorptive neutral density filters to control the amount of power incident on the sample imaged. Then they pass through spatial filters to remove any high spatial frequencies and expand the beams. The 488 nm source reflects off of a dichroic mirror (z488rdc, Chroma Technology Corporation, Rockingham, VT) for fluorescence imaging, and the 811 nm source reflects off of a 50/50 beamsplitter (BSW11, Thorlabs, Newton, NJ) for reflectance imaging.

A custom-designed polygon scanner (Lincoln Laser, Phoenix, AZ) serves as the horizontal fast scan or line scan in the x dimension. The mirror has 14 facets, a scan

angle of 24°, and a maximum speed of 37,500 rotations per minute (RPM).The polygon scanner provides line scan rates from 2.5 kHz to 8.75 kHz. A Keplerian telescope system with 75 mm effective focal length (EFL) (49-389, Edmund Optics, Barrington, NJ) images the illumination source onto the galvanometer scanner (6220HM40B, Cambridge Technologies, Lexington, MA). The galvanometer scanner is the vertical slow scan or frame scan in the y dimension and provides a scan rate up to 15 frames per second (fps). Both scanning mirrors are driven by a data acquisition (DAQ) board (NI PCI-6251, National Instruments, Austin, TX) controlled by LabVIEW software.

Another Keplerian telescope system with 75 mm and 100 mm EFL (49-389, 49-390, Edmund Optics, Barrington, NJ) expands the beam to fill the back aperture of the 40x 0.8NA water immersion microscope objective (MRD07420, Nikon) with 3.5 mm working distance. The beam is focused to a point on the sample. The sample rests on a XYZ motorized stage with 0.05 micron resolution, 100 mm of travel in any axis, and 7 mm/sec maximum speed (KT-LSM100A, Zaber Technologies Inc, Vancouver, British Columbia, Canada).

The fluorescence or reflectance signal is collected by the objective and passes back through the telescope system and is descanned by the scanning mirror combination. If imaging in reflectance mode the signal will pass through the 50/50 beam splitter and the dichroic before approaching the detection arm. When imaging in fluorescence mode, the beam splitter is rotated out of the light path so the fluorescence signal only passes through the dichroic mirror, reducing loss. A removable emission filter (HHQ495LP, Chroma Technology Corporation, Rockingham, VT) is placed after the dichroic to

prevent any unwanted laser light from reaching the detector. The signal is focused onto the pinhole using a lens with 50 mm EFL (NT49-792, Edmund Optics, Barrington, NJ). Various pinhole sizes can be used to optimize signal throughput and resolution. Then another lens with 50 mm EFL (NT49-792, Edmund Optics, Barrington, NJ) refocuses the signal onto a photomultiplier tube (PMT) detector (H9433-03MOD, Hamamatsu, Bridgewater, NJ). Figure 7 shows pictures of the constructed benchtop dual-mode confocal microscope.

Fig. 7. Images of the constructed bench top confocal reflectance and fluorescence microscope.

3.3 Image Formation

To form a 2D image using a point-scanning confocal microscope, the beam must be scanned in two dimensions using scanning mirrors. The PMT records a voltage signal from each point which is assigned to a certain intensity value. A framegrabber (NI PCI 1410, National Instruments, Austin, TX) digitizes the voltage signal and a collection of these points creates a 2D image of the focal plane within the sample so that it may be displayed on a computer monitor in near-real time.

The framegrabber requires three inputs: the signal from the PMT, a horizontal synchronization (HSYNC) input, and a vertical synchronization (VSYNC) input. The HSYNC and VSYNC are synchronization signal that correspond to the polygon and galvanometer scanning mirror positions. The synchronization signals are currently generated in LabVIEW using counter signals.

Confocal mosaicing has recently been used to acquire a large field of view image by capturing individual small field images using scanning mirrors, stepping the sample using a translation stage to scan a larger area, and post-processing the images to reconstruct the large field image [30]. With advancing technology, motorized stages are able to move at faster speeds with high precision and accuracy. A faster way of acquiring an extended image is to use the motorized stage as the frame scan instead of the galvanometer scanning mirror. Combining this imaging method with an automated program to acquire multiple images will help achieve reconstruction of the entire mouse colon much faster than current methods as well as provide a high resolution confocal

image with an extended wide-field of view. Images longer than 2 cm can be acquired, but are currently limited by our framegrabber.

Spectrally encoded confocal microscopy has the potential to acquire in vivo confocal images of the esophagus on the order of 16 cm^2 in approximately 1 minute [31]. Using a broad bandwidth light source with a spectrometer relinquishes the need for fast scanning mechanisms like a polygon mirror. Instead, a rotational fiber scanner is used for scanning. This technique shows promise for transitioning to a fiber-based method for in vivo confocal imaging of the colon.

3.4 Measured Performance

The theoretical lateral resolution, calculated using Eq. (1), for the 488 nm source is 0.37 μm and 0.6 μm for the 811 nm source. Both of these values can be improved or worsened depending on the size of the pinhole used. The theoretical axial resolution, calculated using Eq. (2), for the system is 1.42 μm in fluorescence mode and 2.36 μm in reflectance mode.

Based on the previously mentioned normalized pinhole radius, for $v_p \leq 2.5$, the theoretical pinhole radius should be 2.5 μm for the 488 nm source, and 4 μm for the 811 nm source. The numerical aperture was calculated for the lens in front of the pinhole using the beam diameter and the effective focal length of the lens. The numerical aperture value is 0.078. For my system, based on a 25 μm pinhole diameter, the normalized pinhole radius is 12.6 for the 488 nm source and 7.56 for the 811 nm source.

Lateral resolution was measured by taking an image of a reflective Ronchi grating with 40 line pairs per mm, as seen in Figure 8, then plotting a line profile across

the grating edge shown in Figure 9. The distance between the 10% and 90% intensity values gives the lateral resolution. This method was used to measure the lateral resolution in fluorescence mode and reflectance mode.

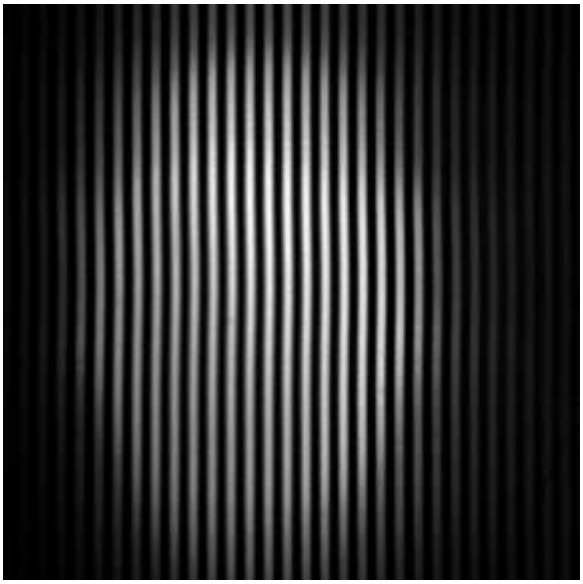

Fig. 8. Ronchi grating with 40 line pairs per mm with 750 x 750 FOV acquired at 8 fps.

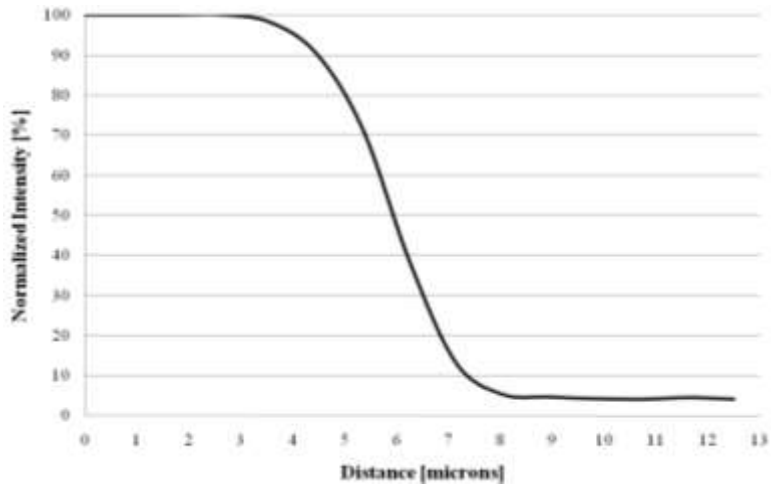

Fig. 9. Line profile across a grating edge showing lateral resolution.

Axial resolution was measured using a reflective silver mirror as the sample and moving it in and out of the focal plane while measuring and recording intensity values passing through the pinhole. A program was written in LabVIEW to automate this process by controlling the motorized stage and recording intensity values from the PMT. The full width half maximum (FWHM) of Figure 10 gives the axial resolution. This was done for both the 488 nm and the 811 nm illumination sources for various pinhole sizes.

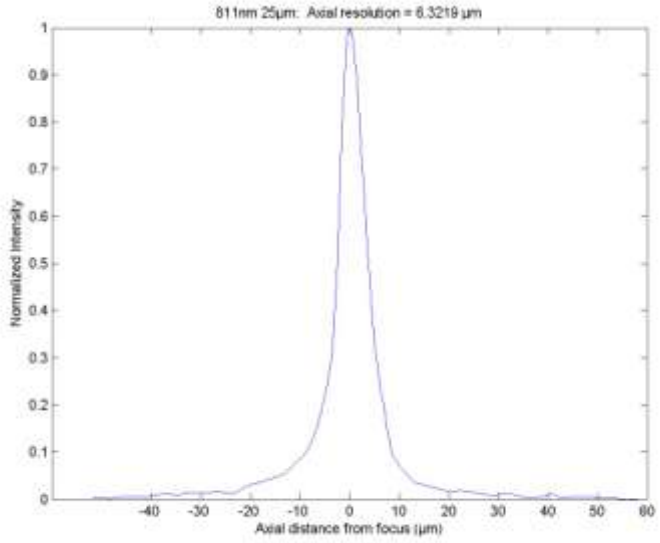

Fig. 10. Normalized intensity as a function of axial distance from the focus of the microscope objective for the 811 nm laser using a 25 micron pinhole. The FWHM is 6 µm.

Table 2 shows a summary of the plotted data for lateral and axial resolution as a function of wavelength and pinhole diameter.

Table 2 Measured lateral and axial resolutions

	Measured Lateral Resolution [µm]		Measured Axial Resolution [µm]	
Pinhole Diameter [µm]	**488 nm**	**811 nm**	**488 nm**	**811 nm**
25	< 2	2	4	6
50	< 2	3	8	13
100	< 4	5	16	19

Acquired image sizes are on the order of 1mm x 1mm. Field of view is measured by imaging a Ronchi grating under the same parameters that an image is acquired. Using ImageJ software, the number of pixels is noted per a 25 micron line pair. This conversion is used to estimate the FOV for acquired images.

Figure 11 shows an image of a fluorescent 1951 Air Force Target taken at 8 fps using the 488 nm laser with a 25µm pinhole. The galvonometer amplitude was fixed at 2.4 volts and the polygon was running at a frequency of 8333.33 Hz. In this image, 1 pixel is equal to 25 µm.

The smallest feature exhibited on the fluorescent 1951 US Air Force target is group 7, element 6 with 228 line pairs per mm.

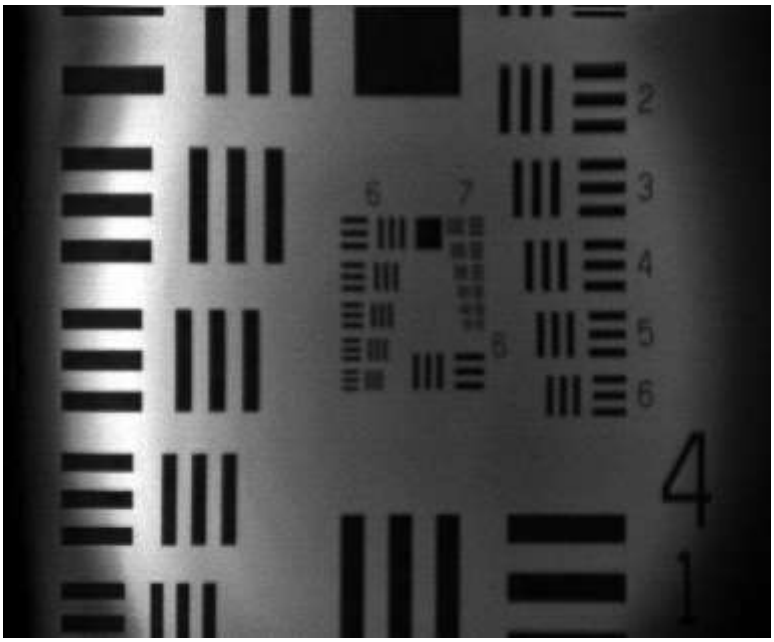

Fig. 11. Fluorescent 1951 US Air Force Target with 865µm x 990 µm FOV using a 25 µm pinhole. Image was acquired at 8fps.

Figure 12 shows another image of an Air Force Target imaged at 15 fps with the galvanometer amplitude fixed at 3.4 volts and the polygon running at a frequency of 8333.33 Hz.

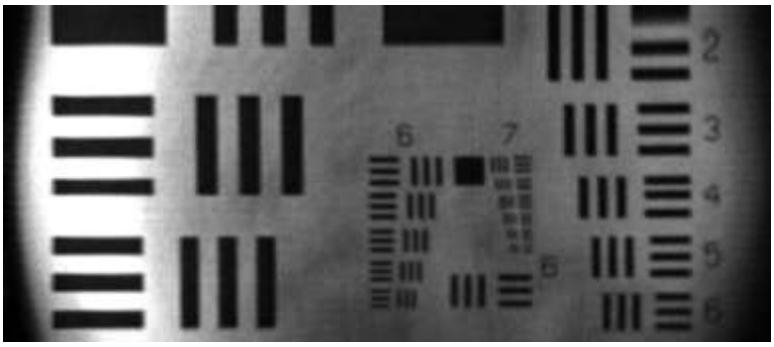

Fig. 12. Fluorescent 1951 US Air Force Target with 400 μm x 900 μm FOV and acquired at 15 fps using a 50 micron pinhole.

The FOV is variable depending on the amplitude provided to the galvanometer. A smaller amplitude for the galvanometer provides an image with similar width in the y-axis as seen in Figure 12. The height is approximately half the size because we are currently limited to a 8333.33 Hz line scan from the polygon scanning mirror.

4. COLON IMAGING

4.1 Mouse Model of Inflammatory Disease

Dextran sodium sulfate (DSS) induces inflammation in mice to model colitis in humans. When used in conjunction with azoxymethane, the mice can develop colon cancer [2]. The DSS solution is added to their drinking water.

Confocal microscopy is commonly used in biology to image cells and tissue slices stained with fluorescent dyes. Imaging bulk colon tissue using confocal reflectance and fluorescence microscopy may provide a better understanding of changes in overall tissue structure without adding distortion due to fixation and slicing of tissue.

4.2 Tissue Preparation and Imaging

Figures 13 and 14 show fluorescence confocal images of normal mouse colon tissue stained with 1 mg/ml AO. These images were taken as preliminary data before doing a comparative study of normal tissue to acute inflammation. All imaging parameters were fixed at a line scan of 8333.33 Hz, a galvanometer amplitude of 3.4 volts, and images were acquired at 15 fps.

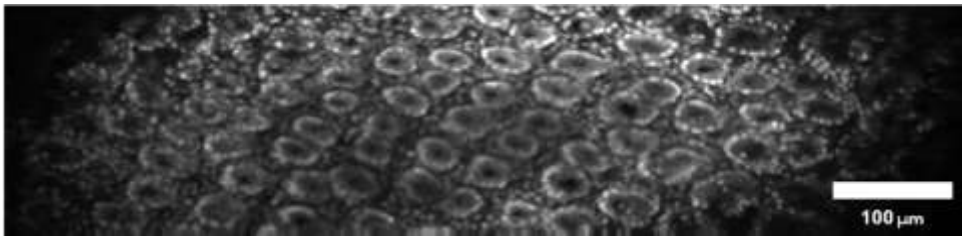

Fig. 13. Fluorescence confocal image of normal mouse colon tissue after application of 1mg/mL of acridine orange with 200 x 800 microns FOV. Acquired at 15 fps. The crypts appear uniform in size with bright nuclei surrounding the crypt openings.

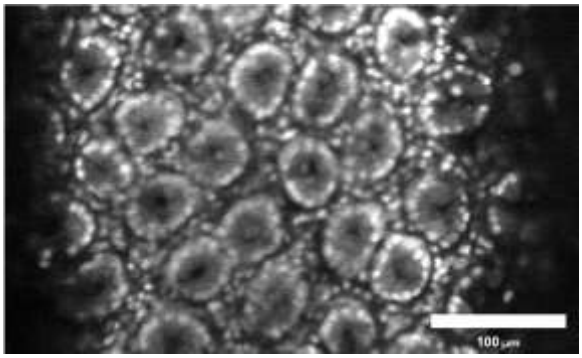

Fig. 14. Fluorescence confocal image of normal mouse colon tissue after application of 1 mg/mL of acridine orange with 250 x 425 microns FOV. Acquired at 15 fps. This is an image near the surface of the mouse colon tissue. Crypt sizes are uniform in size and surrounded by bright nuclei.

For the inflammation study, four mice were used to evaluate the confocal microscope's capability to image normal colon tissue and DSS-induced inflammation. Two mice were used as controls for fluorescence and reflectance imaging. The other two mice are expected to exhibit an onset of inflammation after being treated with 2.5% DSS for five days with a one day recovery period. The mice were approximately 10 weeks old and were fed a regular chow diet. They were all female C57B1/6.

As soon as the mouse colon tissue was acquired for imaging, I opened up the colons by cutting them along a fatty tissue line that travels from the proximal end to the distal end of the colon. The colons are rinsed in two phosphate buffered solution (PBS) washes to remove any fecal matter.

For reflectance imaging, one normal and one inflamed mouse colon are soaked in 5% acetic acid for 30 seconds [18, 32] and then rinsed with PBS for one minute before imaging. For fluorescence imaging, the other two colons are soaked in 1 mg/mL AO for two minutes and rinsed in PBS for one minute. The colons are placed in petri dishes with PBS solution and are imaged individually using the confocal microscope. Figures 15-21 were acquired at 15 fps and are approximately 500 μm x 925 μm in size. Scale bars in all images are 100 μm.

Normal tissue imaged in fluorescence mode is seen in Figures 15, 16, and 17.

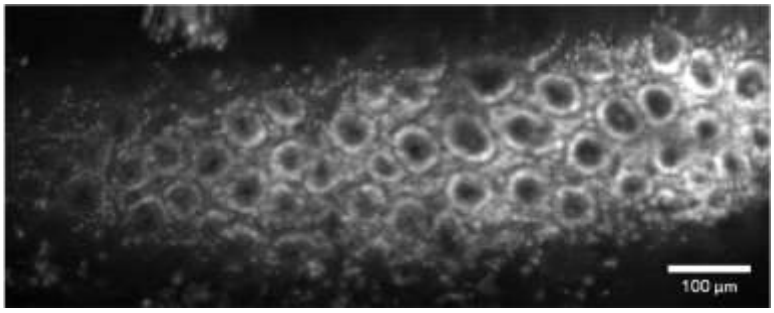

Fig. 15. Fluorescence confocal image of normal mouse colon tissue showing colon crypts uniform in size and surrounded by bright nuclei. Tissue was stained with application of 1 mg/mL of acridine orange for 2 minutes.

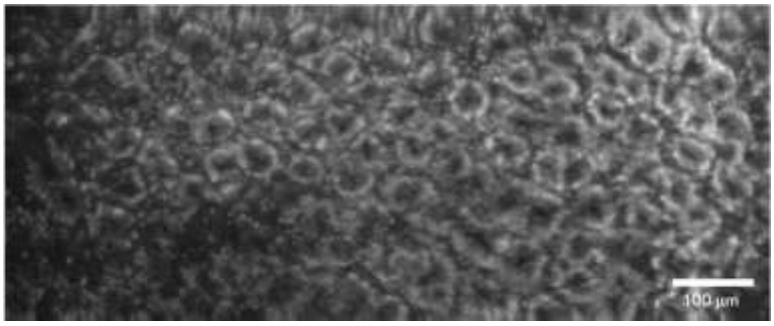

Fig. 16. Fluorescence confocal image of normal mouse colon tissue exhibiting evenly distributed colon crypts. Crypt structures are uniform is size and shape. Tissue was stained with 1 mg/mL of acridine orange.

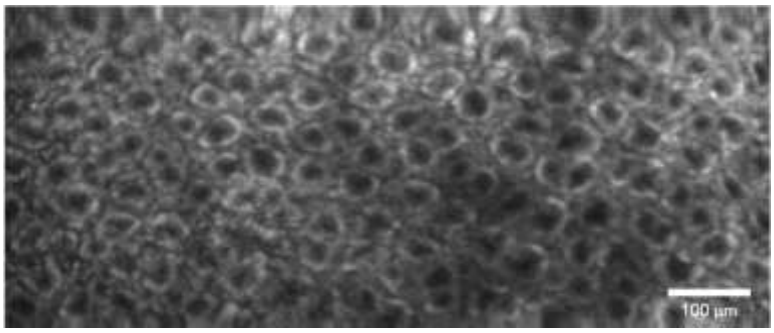

Fig. 17. Fluorescence confocal image of normal mouse colon tissue after application of 1 mg/mL of acridine orange. Crypt structures appear uniform in size and similar in shape.

All of the figures showing normal mouse colon tissue imaged using fluorescence mode exhibit uniform crypt size of 40 - 50 microns and lumen size of 32 microns. The colon crypts are evenly distributed throughout the tissue. As the tissue becomes inflamed as in Figures 18 and 19, the colon crypt lumens no longer appear uniform in size. They are on the order of 17 microns.

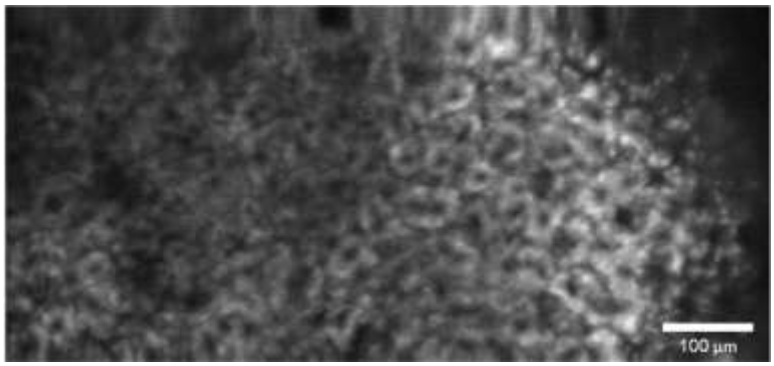

Fig. 18. Fluorescence confocal image of inflamed mouse colon. Tissue was stained with 1 mg/mL of acridine orange. Crypts are not easily identifiable.

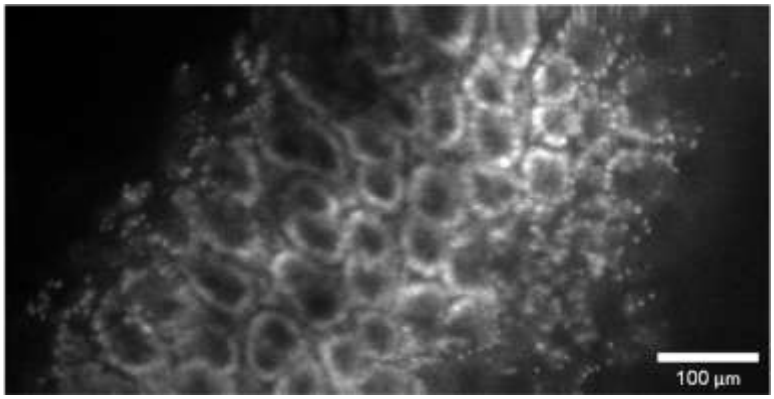

Fig. 19. Fluorescence confocal image near the surface of inflamed mouse colon tissue showing enlarged crypt lumen. Tissue was stained with 1 mg/mL of acridine orange.

Figure 20 shows a reflectance confocal image near the surface of normal mouse colon tissue soaked in 5% acetic acid for 30 seconds. Again, the colon crypts appear uniform in size and distribution throughout the tissue.

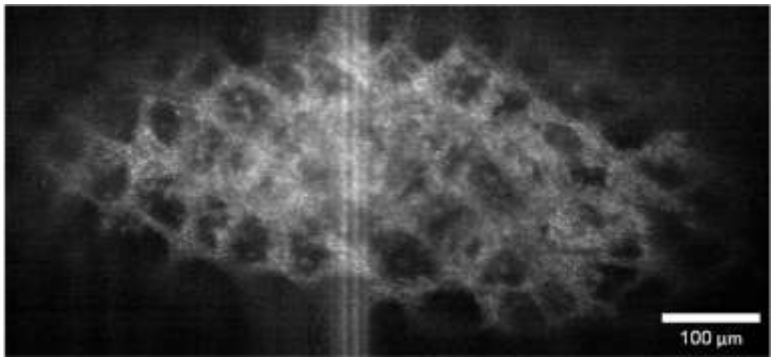

Fig. 20. Reflectance confocal image of normal mouse colon tissue. Image was taken near the surface after application of 5% acetic acid for 30 seconds. Crypts are on the order of 40 – 50 microns.

Inflamed tissue imaged in reflectance mode is seen in Figure 21. This image is also near the surface and the crypts do not appear uniform in size as compared to the normal tissue.

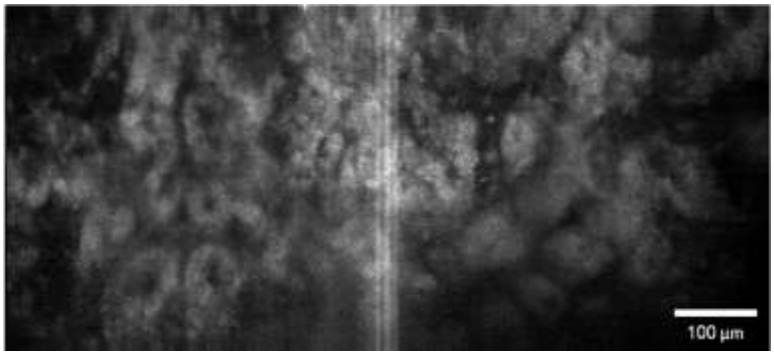

Fig. 21. Reflectance confocal image of inflamed mouse colon tissue. Image was acquired after application of 5% acetic acid for 30 seconds.

By fixing the galvanometer and using the motorized translation stage as the frame scan, we are able to acquire images approximately1 mm x 2 cm in 2 seconds at various depths within the tissue. The acquired images are single frames that do not require any form of mosaic tiling or post-processing. The confocal resolution is also maintained throughout the image providing a high-resolution, wide-field extended image. Figure 22 exhibits extended images of a reflective Ronchi grating (left-middle) and normal mouse colon tissue (right-middle) acquired near the surface. The magnified images along the sides indicate that there is not a loss in resolution.

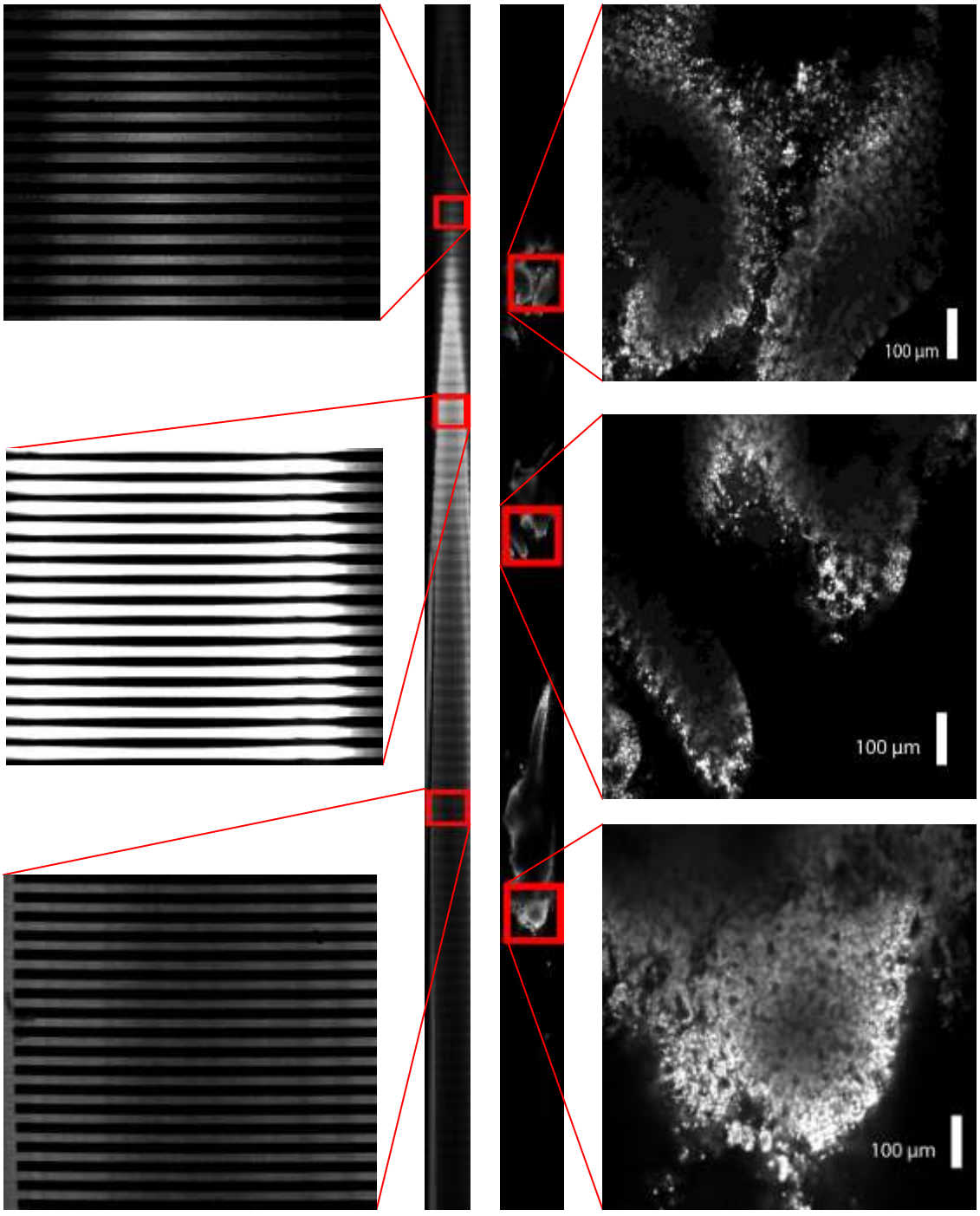

Fig. 22. Magnified views along the sides show the ability to resolve nuclei and colon crypts within the extended confocal image. The images are approximately 1 mm by 2 cm FOV. The left-middle image is an image of a reflective Ronchi grating, 1000 x 29000 pixels. The right-middle image is a fluorescence confocal image of normal mouse colon tissue, 1500 x 29000 pixels.

4.3 Comparison to Histology

After the imaging process is completed, the samples are prepared for histology. The samples are individually rolled from proximal to distal end using a special histology paper that does not disintegrate in ethanol (EtOH). This technique is known as a Swiss roll [33]. Performing histology in this manner provides histology information along the length of the whole colon rather than a section.

The tissue is stored in 70% EtOH overnight at 4° C to dehydrate the tissue. Then the histology paper is removed the next day and the tissue is rolled again before returning to 70% EtOH until histology preparation. After dehydration, the tissue is embedded into a mold which is hardened before sectioning the tissue. The tissue is stained with hematoxylin and eosin to provide contrast. Hematoxylin stains the nuclei blue and eosin stains the surrounding cytoplasm pink. All images were taken with a 20x microscope objective and are approximately 440 μm x 330 μm FOV.

In Figure 23, the colon crypts appear to have uniform spacing throughout the tissue and are of similar depth. This corresponds well with the acquired fluorescence confocal image of the normal mouse colon.

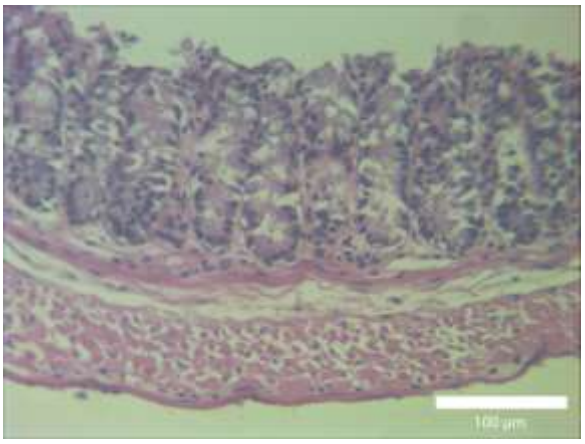

Fig. 23. Transverse histology image of normal mouse colon tissue used for fluorescence imaging. The colon crypts appear to be uniform in size and evenly spaced throughout the tissue.

The inflamed tissue shown in Figure 24 appears distorted with a loss of tissue architecture. Correlating with the previously shown confocal image, the colon crypts do not appear to be uniform in size at the surface of the tissue.

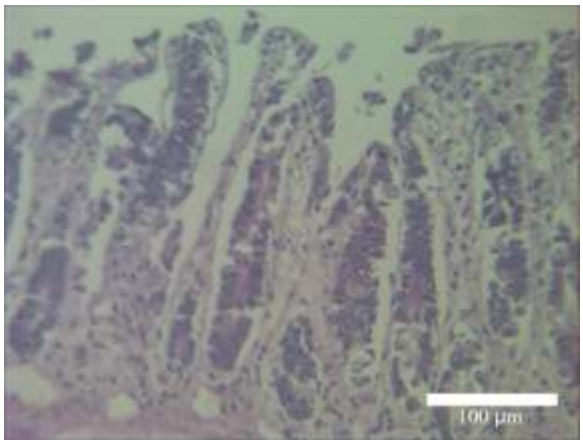

Fig. 24. Transverse histology image of inflamed mouse colon tissue used for fluorescence imaging. The colon crypts no longer appear to have a uniform distribution throughout the tissue. There is a loss of architecture in the colon tissue.

The normal tissue shown in Figure 25 shows a uniform crypt size and distribution along the colon as seen in the corresponding reflectance confocal image of normal mouse colon tissue.

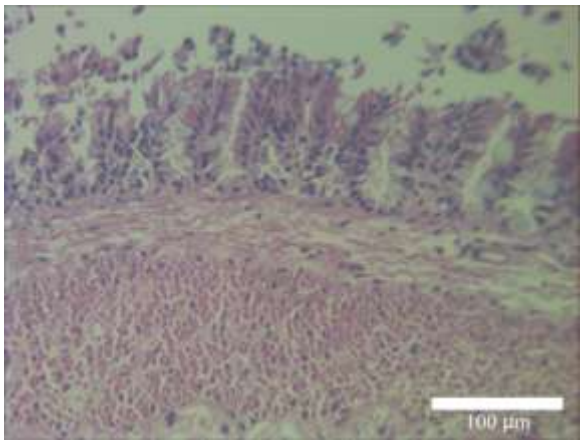

Fig. 25. Transverse histology image of normal mouse colon tissue used for reflectance imaging. The colon crypts appear uniform in size and spacing.

The inflamed tissue seen in Figure 26 does not clearly show the crypt openings at the surface of the tissue correlating once again correlating with the acquired reflectance confocal image of the inflamed mouse colon.

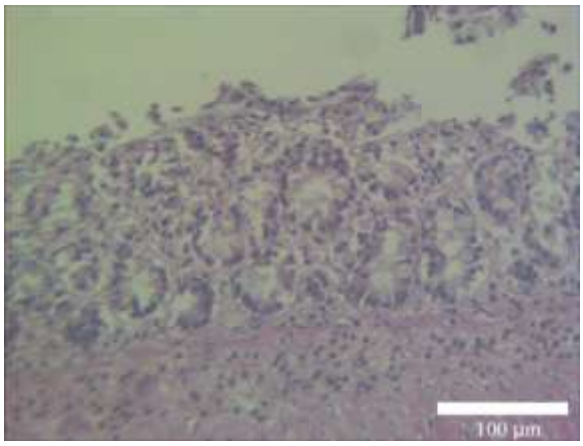

Fig. 26. Transverse histology image of inflamed mouse colon tissue used for reflectance imaging. There is a distinct loss of structure and architecture in this image. The colon crypts do not appear uniform in size.

5. SUMMARY AND CONCLUSIONS

5.1 Summary

The objective of this research is to evaluate the ability of a dual-mode confocal microscope to characterize structural and molecular changes in mouse colon tissue as inflammation and cancer develop. I have completed the first specific aim by designing and constructing a reflectance and fluorescence confocal microscope for imaging of the mouse colon. The second specific aim was to image colon tissue of healthy mice and mice with induced inflammatory bowel disease then compare these images to corresponding histology images. The confocal images correlate well with the histology images revealing comparable characteristic features such as colon crypt size and distribution throughout the tissue.

The system specifications meet the design requirements and in some cases, such as the field of view, exceed original expectations. The lateral resolution of the system is 3 μm for the 488 nm laser source and for the 811 nm laser source. The axial resolution is 4 μm for the 488 nm laser source and 6 μm for the 811 nm laser source. Field of view is approximately 1mm x 1mm with an acquisition of 8fps. When imaging in fluorescence mode the penetration depth in mouse colon tissue is approximately 150 μm.

This reflectance and fluorescence confocal microscope is capable of resolving nuclei and colon crypts in normal and inflamed mouse colon tissue. Clear differences are seen between the two by observing colon crypt size and distribution throughout the tissue. In normal tissue the colon crypts are uniform in size and distribution along the

colon. As the tissue becomes inflamed, the colon crypts are no longer uniform in size and tissue architecture is lost.

5.2 Conclusions

The confocal system we built and will continue to modify has the ability to help those who are already diagnosed with colon cancer and can also screen people who may be at risk of developing this disease. An optical biopsy of thick specimens does not require tissue to be fixed or sliced for imaging and therefore provides a means for a much faster diagnosis of tissue. A correlation is seen between confocal and histology images indicating potential for immediate diagnostic evaluation. When performed in vivo, the number of random biopsies needed would be greatly reduced and be less stressful on the patient. This instrument shows the capability for imaging inflammation in the mouse colon and exhibits potential for future use as a diagnostic tool in optical biopsy.

5.3 Future Work

Future plans for this system include the addition of another laser source. The system currently has a single wavelength for fluorescence imaging. I would like to add another wavelength so I can utilize other exogenous fluorophores like cresyl violet for colon tissue imaging. The bench top system will also be condensed to a cart so it is portable throughout departments and labs on campus.

Additionally, I plan to perform mosaicing of the entire mouse colon for a more complete study of the effects of inflammation. I would like to image chronic inflammation on my system and compare it to images of acute inflammation that I will

acquire for this thesis proposal. Acute inflammation is induced over a period of 5 days with 2.5% DSS treatment. There is a one day recovery before I get the colon tissue for imaging. Chronic inflammation is more of a long term study that is done over 2 months. The mice are treated with 2.5% DSS for 4-5 days. They are treated 3 times with a recovery period between treatments.

In order to characterize image features of normal, inflamed, precancerous, and cancerous tissue, I plan to develop a method to quantitatively analyze image features observed in my confocal images of mouse colon tissue. This process may include developing an algorithm for counting colon crypts observed in the tissue and then comparing values along different parts of the colon as well as between different classifications of the state of the tissue.

Finally, the system will be modified to a fiber-based reflectance confocal system for in vivo imaging. The system will be completely noninvasive, therefore exogenous stains will not be used and tissue will not have to be excised, so treatment could be monitored over time. My current system has to be modified to have a flexible endoscope, utilizing a fiber bundle raster scanned at the proximal tip. The optical fibers are placed in a conjugate image plane to the focal plane of the confocal microscope. I will modify the scan lens to couple light into the fibers and design a custom miniature objective lens. The miniature objective will transmit the illumination from the distal end of the fiber to the colon tissue, and it will also collect the reflectance signal from within the tissue and image it back onto the distal end of the fiber bundle [34]. The illumination source will be coupled into one fiber at a time and will serve as both the point source

illumination fiber and pinhole collection fiber. The other fibers in the bundle may collect some of the out of focus light, but a pinhole located in front of the PMT detector will reject this unwanted signal [35].

REFERENCES

1. S. H. Itzkowitz and X. Y. Yio, "Inflammation and cancer - IV. Colorectal cancer in inflammatory bowel disease: the role of inflammation," American Journal of Physiology-Gastrointestinal and Liver Physiology **287**, G7-G17 (2004).

2. Q. Jia, J. R. Lupton, R. Smith, B. R. Weeks, E. Callaway, L. A. Davidson, W. Kim, Y. Y. Fan, P. Yang, R. A. Newman, J. X. Kang, D. N. McMurray, and R. S. Chapkin, "Reduced colitis-associated colon cancer in Fat-1 (n-3 fatty acid desaturase) transgenic mice," Cancer Res **68**, 3985-3991 (2008).

3. D. K. Podolsky, "Inflammatory bowel disease," N Engl J Med **347**, 417-429 (2002).

4. R. Kiesslich, A. Hoffman, M. Goetz, S. Biesterfeld, M. Vieth, P. R. Galle, and M. F. Neurath, "In vivo diagnosis of collagenous colitis by confocal endomicroscopy," Gut **55**, 591-592 (2006).

5. A. Hoffman, M. Goetz, M. Vieth, P. R. Galle, M. F. Neurath, and R. Kiesslich, "Confocal laser endomicroscopy: technical status and current indications," Endoscopy **38**, 1275-1283 (2006).

6. H. S. Cooper, S. N. Murthy, R. S. Shah, and D. J. Sedergran, "Clinicopathologic study of dextran sulfate sodium experimental murine colitis," Lab Invest **69**, 238-249 (1993).

7. T. Tanaka, H. Kohno, R. Suzuki, Y. Yamada, S. Sugie, and H. Mori, "A novel inflammation-related mouse colon carcinogenesis model induced by azoxymethane and dextran sodium sulfate," Cancer Sci **94**, 965-973 (2003).

8. K. Sokolov, K. B. Sung, T. Collier, A. Clark, D. Arifler, A. Lacy, M. Descour, and R. Richards-Kortum, "Endoscopic microscopy," Dis Markers **18**, 269-291 (2002).

9. American Cancer Society Colorectal Cancer Guide, *Colon and Rectum Cancer,* (American Cancer Society, 2009). http://www.cancer.org/Cancer/ColonandRectumCancer/DetailedGuide/index

10. W. Strober, I. Fuss, and P. Mannon, "The fundamental basis of inflammatory bowel disease," J Clin Invest **117**, 514-521 (2007).

11. R. Kiesslich, J. Burg, M. Vieth, J. Gnaendiger, M. Enders, P. Delaney, A. Polglase, W. McLaren, D. Janell, S. Thomas, B. Nafe, P. R. Galle, and M. F.

Neurath, "Confocal laser endoscopy for diagnosing intraepithelial neoplasias and colorectal cancer in vivo," Gastroenterology **127**, 706-713 (2004).

12. C. A. Seldenrijk, B. C. Morson, S. G. Meuwissen, N. W. Schipper, J. Lindeman, and C. J. Meijer, "Histopathological evaluation of colonic mucosal biopsy specimens in chronic inflammatory bowel disease: diagnostic implications," Gut **32**, 1514-1520 (1991).

13. J. T. C. Liu, M. J. Mandella, S. Friedland, R. Soetikno, J. M. Crawford, C. H. Contag, G. S. Kino, and T. D. Wang, "Dual-axes confocal reflectance microscope for distinguishing colonic neoplasia," J Biomed Opt **11**, 054019 (2006).

14. O. Watanabe, T. Ando, O. Maeda, M. Hasegawa, D. Ishikawa, K. Ishiguro, N. Ohmiya, Y. Niwa, and H. Goto, "Confocal endomicroscopy in patients with ulcerative colitis," Journal of Gastroenterology and Hepatology **23**, S286-S290 (2008).

15. A. L. Carlson, L. G. Coghlan, A. M. Gillenwater, and R. R. Richards-Kortum, "Dual-mode reflectance and fluorescence near-video-rate confocal microscope for architectural, morphological and molecular imaging of tissue," J Microsc **228**, 11-24 (2007).

16. T. Wilson and A. R. Carlini, "Size of the detector in confocal imaging systems," Opt Lett **12**, 227-229 (1987).

17. P. M. Delaney, R. G. King, J. R. Lambert, and M. R. Harris, "Fibre optic confocal imaging (FOCI) for subsurface microscopy of the colon in vivo," J Anat **184** (Pt 1), 157-160 (1994).

18. D. S. Gareau, Y. G. Patel, Y. Li, I. Aranda, A. C. Halpern, K. S. Nehal, and M. Rajadhyaksha, "Confocal mosaicing microscopy in skin excisions: a demonstration of rapid surgical pathology," Journal of Microscopy-Oxford **233**, 149-159 (2009).

19. Y. G. Patel, K. S. Nehal, I. Aranda, Y. Li, A. C. Halpern, and M. Rajadhyaksha, "Confocal reflectance mosaicing of basal cell carcinomas in Mohs surgical skin excisions," J Biomed Opt **12**, 034027 (2007).

20. M. Rajadhyaksha, R. R. Anderson, and R. H. Webb, "Video-rate confocal scanning laser microscope for imaging human tissues in vivo," Appl Opt **38**, 2105-2115 (1999).

21. P. Kim, M. Puoris'haag, D. Cote, C. P. Lin, and S. H. Yun, "In vivo confocal and multiphoton microendoscopy," J Biomed Opt **13**, 010501 (2008).

22. J. B. Pawley, *Handbook of Biological Confocal Microscopy,* Third ed. (Springer, 2006).

23. M. Müller, *Introduction to Confocal Fluorescence Microscopy,* Vol. TT69, Second ed. (SPIE, 2006).

24. T. Collier, P. Shen, B. de Pradier, K. B. Sung, R. Richards-Kortum, M. Follen, and A. Malpica, "Near real time confocal microscopy of amelanotic tissue: dynamics of aceto-whitening enable nuclear segmentation," Opt Express **6**, 40-48 (2000).

25. T. Collier, A. Lacy, R. Richards-Kortum, A. Malpica, and M. Follen, "Near real-time confocal microscopy of amelanotic tissue: detection of dysplasia in ex vivo cervical tissue," Acad Radiol **9**, 504-512 (2002).

26. S. Yoshida, S. Tanaka, M. Hirata, R. Mouri, I. Kaneko, S. Oka, M. Yoshihara, and K. Chayama, "Optical biopsy of GI lesions by reflectance-type laser-scanning confocal microscopy," Gastrointestinal Endoscopy **66**, 144-149 (2007).

27. W. McLaren, P. Anikijenko, D. Barkla, T. P. Delaney, and R. King, "In vivo detection of experimental ulcerative colitis in rats using fiberoptic confocal imaging (FOCI)," Dig Dis Sci **46**, 2263-2276 (2001).

28. H. W. Wang, J. Willis, M. I. Canto, M. V. Sivak, Jr., and J. A. Izatt, "Quantitative laser scanning confocal autofluorescence microscopy of normal, premalignant, and malignant colonic tissues," IEEE Trans Biomed Eng **46**, 1246-1252 (1999).

29. R. Drezek, K. Sokolov, U. Utzinger, I. Boiko, A. Malpica, M. Follen, and R. Richards-Kortum, "Understanding the contributions of NADH and collagen to cervical tissue fluorescence spectra: modeling, measurements, and implications," J Biomed Opt **6**, 385-396 (2001).

30. D. S. Gareau, Y. B. Li, B. Huang, Z. Eastman, K. S. Nehal, and M. Rajadhyaksha, "Confocal mosaicing microscopy in Mohs skin excisions: feasibility of rapid surgical pathology," J Biomed Opt **13**, 054001 (2008).

31. D. Yelin, C. Boudoux, B. E. Bouma, and G. J. Tearney, "Large area confocal microscopy," Opt Lett **32**, 1102-1104 (2007).

32. R. A. Drezek, T. Collier, C. K. Brookner, A. Malpica, R. Lotan, R. R. Richards-Kortum, and M. Follen, "Laser scanning confocal microscopy of cervical tissue before and after application of acetic acid," American Journal of Obstetrics and Gynecology **182**, 1135-1139 (2000).

33. C. Moolenbeek and E. J. Ruitenberg, "The "Swiss roll": a simple technique for histological studies of the rodent intestine," Lab Anim **15**, 57-59 (1981).

34. A. R. Rouse, A. Kano, J. A. Udovich, S. M. Kroto, and A. F. Gmitro, "Design and demonstration of a miniature catheter for a confocal microendoscope," Appl Opt **43**, 5763-5771 (2004).

35. K. B. Sung, C. N. Liang, M. Descour, T. Collier, M. Follen, and R. Richards-Kortum, "Fiber-optic confocal reflectance microscope with miniature objective for in vivo imaging of human tissues," IEEE Transactions on Biomedical Engineering **49**, 1168-1172 (2002).

VITA

Meagan Alyssa Saldua was born in Houston, Texas, on December 15, 1985, to Martin and Irma Saldua. She grew up in Stafford, Texas, and attended Stafford Municipal School District. Meagan received her Bachelor of Science degrees in applied physics and mathematics from Angelo State University in May 2008. She entered the biomedical engineering program at Texas A&M University in August 2008. Her research, under the supervision of Dr. Kristen Maitland, focused on confocal microscopy.

Ms. Saldua may be reached at Texas A&M University, 3120 TAMU, College Station, TX 77843-3120. Her email is meagansaldua@gmail.com.